Supplement of Atmos. Chem. Phys., 22, 1035–1057, 2022
https://doi.org/10.5194/acp-22-1035-2022-supplement


Atmospheric Chemistry and Physics
Open Access
EGU

*Supplement of*

# Atmospheric measurements at Mt. Tai – Part II: HONO budget and radical ($RO_x + NO_3$) chemistry in the lower boundary layer

**Chaoyang Xue et al.**

*Correspondence to:* Chaoyang Xue (chaoyang.xue@cnrs-orleans.fr, 86chaoyang.xue@gmail.com) and Yujing Mu (yjmu@rcees.ac.cn)

## Contents

### Text



### Figures

## S1. Lifetimes of HONO and $NO_x$ and direct HONO emissions ($HONO_{emi}$)

As discussed in the main text (Section 3.2.2.1), the contribution of direct emission on the observed HONO could be overestimated when using a constant $\Delta HONO/\Delta NO_x$ during the daytime due to the distinctly different lifetimes of HONO ($\tau(HONO)$) and $NO_x$ ($\tau(NO_x)$). Therefore, during the daytime, when $\tau(HONO)$ was shorter than 1 h, $HONO_{emi}$ was corrected by multiplying the ratio of $\tau(HONO)/\tau(NO_x)$ (see (Eq-3) in the main text). $\tau(HONO)$ against OH and photolysis was directly obtained from F0AM model simulations (Wolfe et al., 2016). $\tau(NO_x)$ depends on the $NO_2$ lifetime and $NO/NO_2$ ratio regarding the net loss of $NO_x$ is mainly in the form of $HNO_3$ produced through OH or $NO_3$ induced reactions. The equation is shown in (Eq-S1) (Seinfeld and Pandis, 2016).

$$\tau(NO_x) = \tau(NO_2) * (1 + \frac{NO}{NO_2}), \quad \text{(Eq-S1)}$$

Net $NO_2$ loss was through reactions of $NO_2 + OH \rightarrow HNO_3$, $NO_3 + VOCs \rightarrow HNO_3$, and $NO_3 + NO_2 + \text{wet surface} \rightarrow HNO_3$, which were considered to calculate $\tau(NO_2)$. Results on $HNO_3$ production rate are presented in Figure 12 and discussed in Section 3.3.3.2 of the main text. Results on daytime $\tau(HONO)$, $\tau(NO_x)$, and $HONO_{emi}$ were shown in Figure S6.

## S2. A detailed explanation for the MLH employed

A proper level of the employed MLH is of significant importance for parameterizing ground-derived HONO sources, as discussed in Section 3.2.2.4 of the main text. Currently, some studies with ground measurements directly used the boundary layer height (BLH, 1-2 km at noon) instead of MLH. This would largely underestimate the contribution of ground-derived sources, leading to the misunderstanding of HONO formation. In the present study, we could not conclude that the MLH of 50 m (and sensitivity tests for 35-100 m) is the best, but it significantly reduces the uncertainties compared to the use of BLH. Additionally, a reasonable MLH for model study on ground HONO measurements should be in the range we tested. See the explanation below.

Here we assume that the ground surface is the main source of HONO in the atmosphere. This is for example confirmed by recent MAX-DOAS studies (Garcia-Nieto et al., 2018; Ryan et al., 2018; Wang et al., 2019; Xing et al., 2021), in which strong gradients were observed in the lower daytime atmosphere. The gradients can be explained by fast photolysis of HONO during the vertical updraft from the ground surfaces (source region of HONO) during the daytime. The mixing layer higher (MLH), i.e., the height to which ground surface produced HONO will be transported, will depend on both the photolytic lifetime of HONO (inverse of J(HONO)) and the vertical mixing of the atmosphere described e.g., by the eddy-diffusion coefficient. In response to the solar zenith angle (SZA), the lifetime of HONO will decrease from morning to noon, which will solely lead to a decreasing MLH. In contrast, caused by the increasing turbulence from morning to noon (Jacob, 1999), the vertical transport of HONO will increase (increasing MLH). If the vertical transport is increasing in the same way as the photolytic lifetime of HONO is decreasing, both effects will exactly compensate leading to a constant MLH as used for simplicity in the present study.

Generally, the MLH could be defined as the height where the HONO concentration – or more precisely the excess HONO concentration exceeding (height-dependent) $HONO_{PSS}$ – has decreased to 1/e from its ground surface concentration. Caused by the gradients, a formal source determined from the excess over PSS will be height dependent and stronger when measured close to the ground as done in the present study. The reason for this problem is that the sources are not correctly implemented as flux from the ground surface (molecules $m^{-2}$ $s^{-1}$) in a 1D vertical model, but are mathematically treated as a gas phase source in a homogeneously mixing box model, which we used here for simplicity. Thus, the box height has to be even lower than the above-defined MLH and will be better described by the height where the HONO mixing ratio is decreasing to lower values than the measured near the ground surface. A better definition of the height used would be the homogeneous mixing height of the 0D box, for which we used the term MLH for simplicity.

Then we did several steps to scale the MLH used in this study.

A minimum MLH of 35 m was derived based on the assumption that all the $P_{unknown}$ could be wholly explained by photosensitized heterogeneous $NO_2$ reaction on the ground surface in our recent study (Xue et al., 2021).

To scale the maximum of the MLH of HONO, theoretically, the vertical turbulence process within the lifetime of HONO should be considered. For instance, Zhang et al. (2009) estimated the maximum vertical transport distance by turbulent diffusion (Jacob, 1999). A maximum of 350 m at noontime that HONO could reach was obtained. Therefore, MLH for HONO should be much lower than 350 m, which is in agreement with vertical measurements.

Brown et al. (2013) and Vandenboer et al. (2013) both resulted from the same project of Nitrogen, Aerosol Composition, and Halogens on a Tall Tower (NACHTT-11) and the latter one was focused on HONO formation. Vandenboer et al. (2013) conducted similar model simulations with a model height of 150 m. They found significant underestimation in HONO levels, which was attributed to the higher model height compared to the measurement height of 20 m. Hence, to model measurements near the ground surface, a lower MLH than 150 m is needed.

Vertical measurements can further constrain the MLH. A declining HONO trend with altitude was frequently observed in previous vertical measurements (Kleffmann et al., 2003; Meng et al., 2020; Vandenboer et al., 2013; Vogel et al., 2003; Xing et al., 2021; Ye et al., 2018; Zhang et al., 2009). We would like to take the measurements in Germany (Vogel et al., 2003), the USA (Vandenboer et al., 2013) and China (Xing et al., 2021) as examples to scale the MLH. From the ground level (4-10 m) to 100 m above the ground surface, Vogel et al. (2003), Vandenboer et al. (2013), and Xing et al. (2021) observed declining HONO levels from ~0.6 to 0.3 (a representative case from Figure 4), from 0.6 to 0.3 (case from Figure 8), and from 4.8 to 1.6 ppbv (case from Figure 5), respectively. All of those cases suggest that near-ground surface measurements were more weighted by ground-derived sources. Moreover, this phenomenon was observed during their whole campaigns including daytime and nighttime, suggesting a similar level of MLH. Hence, a maximum MLH of 100 m appears appropriate for interrpretation near-ground surface measurements.

In summary, 0-D modeling with the utilization of ~50 m level could represent a general MLH for studying HONO measurements near the ground surface. Nevertheless, we still should highlight that accompanied efforts, e.g., performing sensitivity tests, should always be made to underline the uncertainties.

Regrading deriving MLH from vertical measurements like Xing et al. (2021), we need to conduct 1D modeling simulations with reasonable transport and a real surface flux of HONO. The model results should be compared with near-ground surface measurements or gradient measurements. However, currently, we don't have the tool of a 1D model and gradient measurements. Instead, in this study, we tried to scale the MLH using the above methods, which significantly improved the model performance.

**Figures**

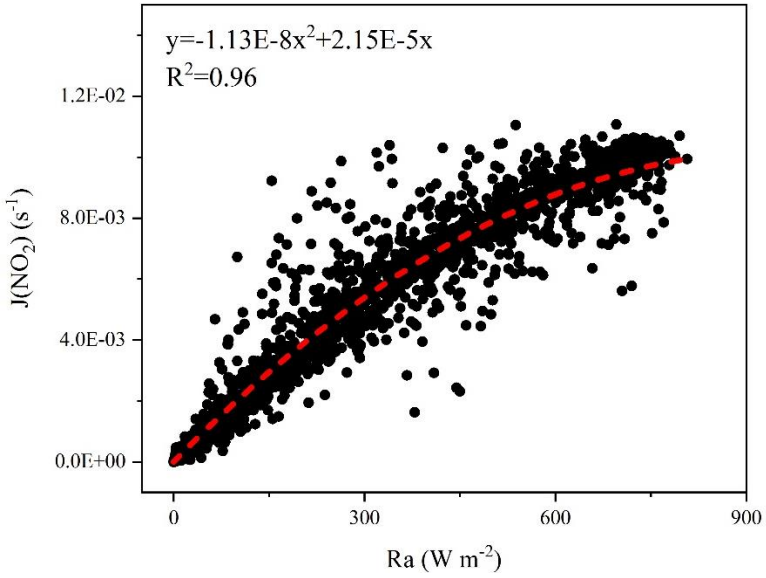


**Figure S1: Correlation between the measured J($NO_2$) and solar irradiance (Ra).**

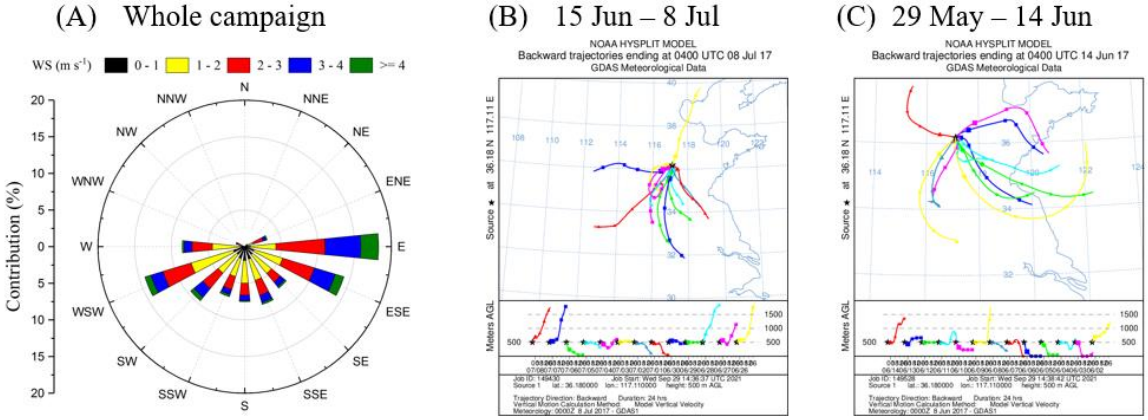


**Figure S2: (A): Wind rose plot for the wind measurements at the foot of Mt. Tai; (B) and (C): 1-day back trajectories from HYSPLIT (https://www.ready.noaa.gov/HYSPLIT.php).**

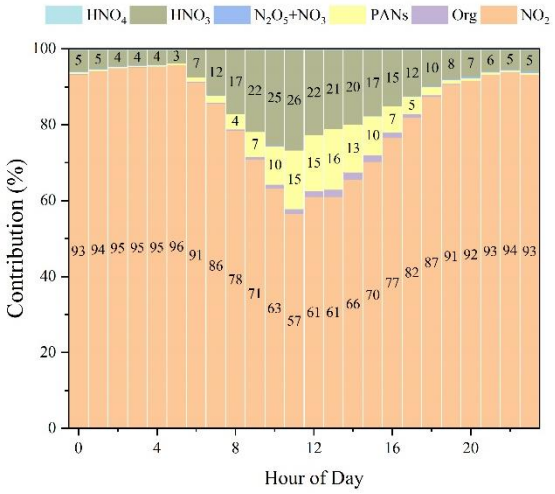


**Figure S3: Relative contribution of each $NO_2^*$ species. PANs = PAN + PPN + MPAN, and Org represents organic nitrates$^*$ ($RONO_2$ + $ROONO_2$).**

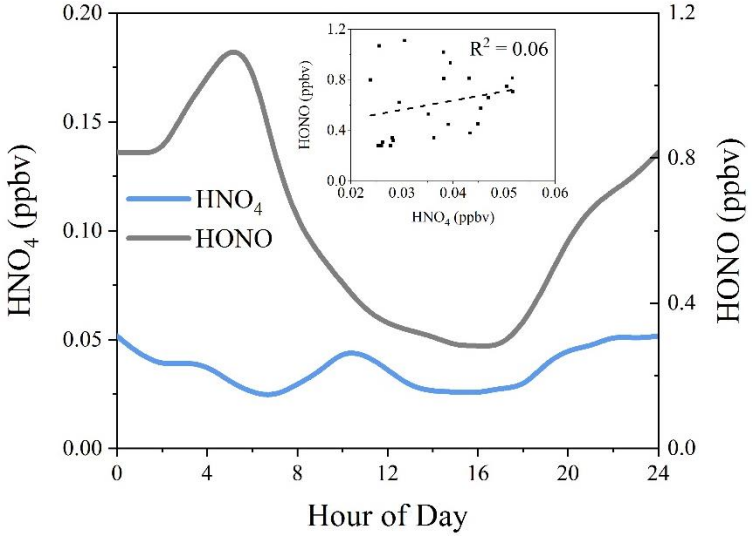


**Figure S4: Diurnal variations of HONO and $HNO_4$ and their correlations.**

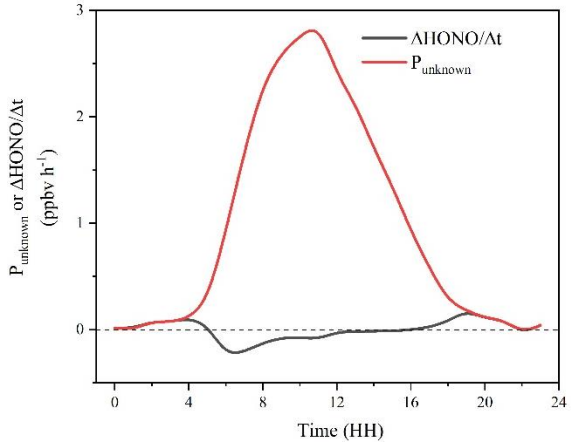


140

**Figure S5: Diurnal variations of $P_{unknown}$ and ΔHONO/Δt.**

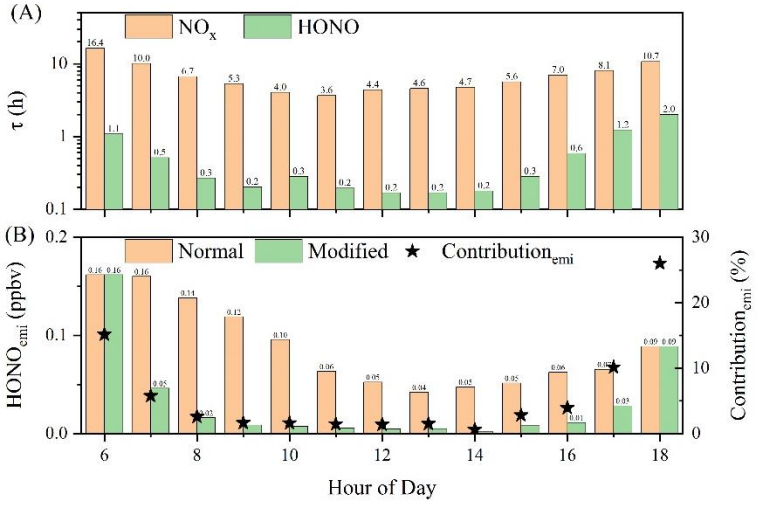


**Figure S6: (A): Daytime lifetimes of HONO and $NO_x$; (B): $HONO_{emi}$ with a constant $\Delta HONO/\Delta NO_x$ ratios (Normal) or modified according to the different lifetimes of HONO and $NO_x$ (Modified) and the contribution of modified $HONO_{emi}$ to the observed HONO.**

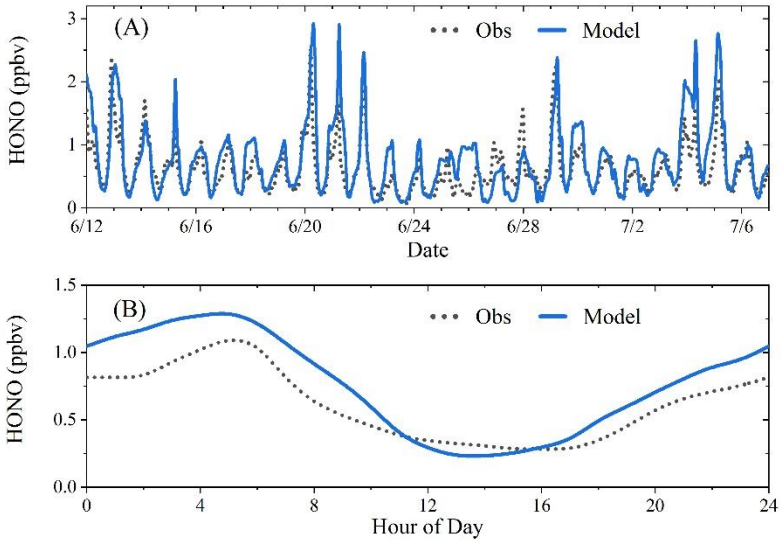


**Figure S7: Modeled (Sce-3 with reduced $\gamma_g$ and enlarged $\gamma_a$ of $1.2\times10^{-3}$) HONO mixing ratios (Model, in blue) in comparison with observations (Obs, in black). (A): time series; (B): average diurnal variations.**

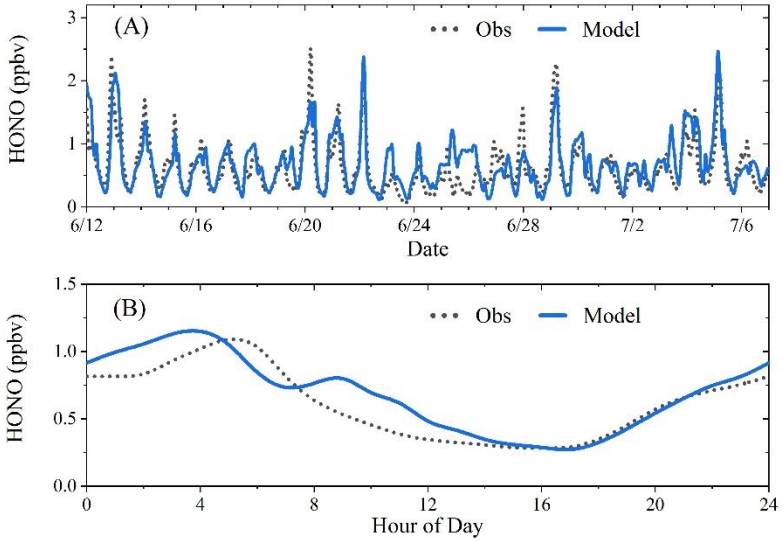


**Figure S8: Modeled (Sce-3 with reduced $\gamma_g$ and enlarged EF of 400) HONO mixing ratios (Model, in blue) in comparison with observations (Obs, in black). (A): time series; (B): average diurnal variations.**

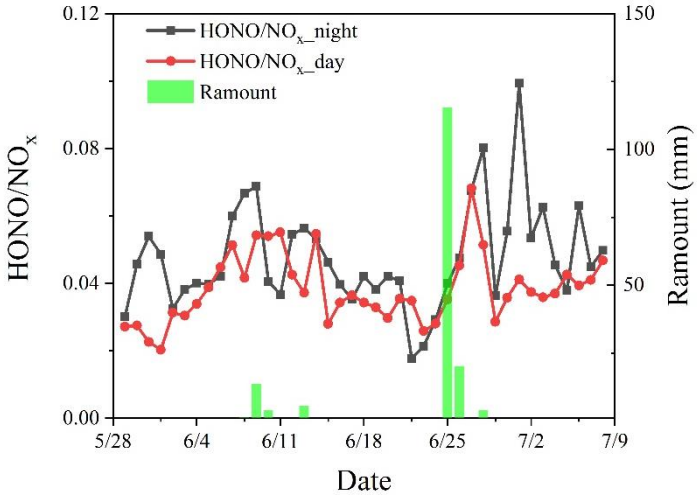


**Figure S9: Daily rainfall amount (Ramount) and daytime and the night-time HONO/$NO_x$.**

155

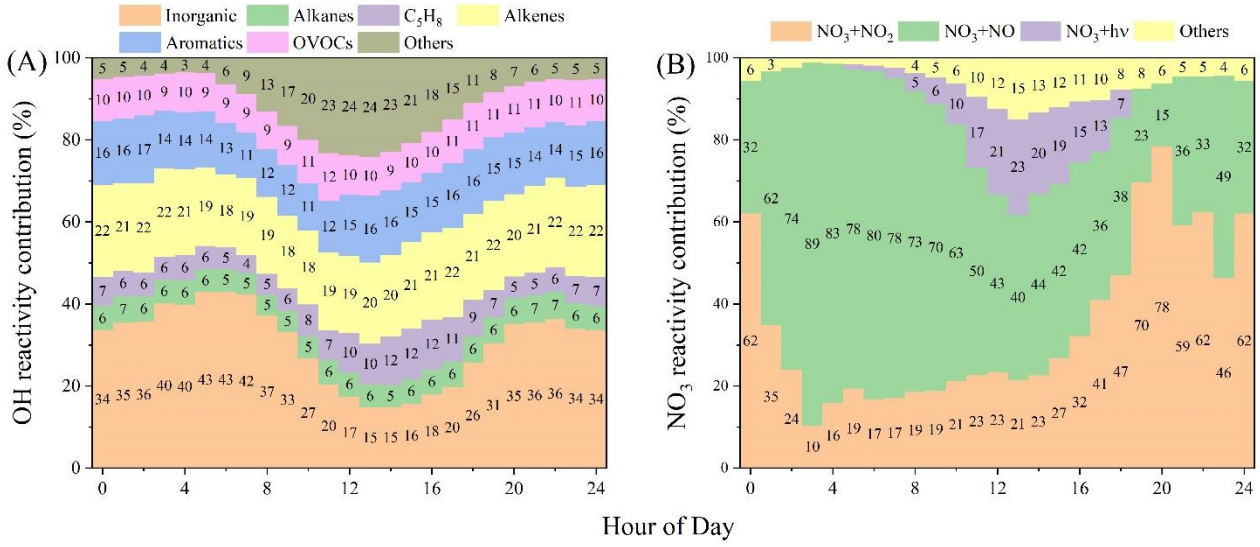


**Figure S10: (A): OH and (B): $NO_3$ reactivity contributions. Reactivity with other unmeasured species was classified as "other". Note that Alkenes do not include $C_5H_8$ which is separately shown.**

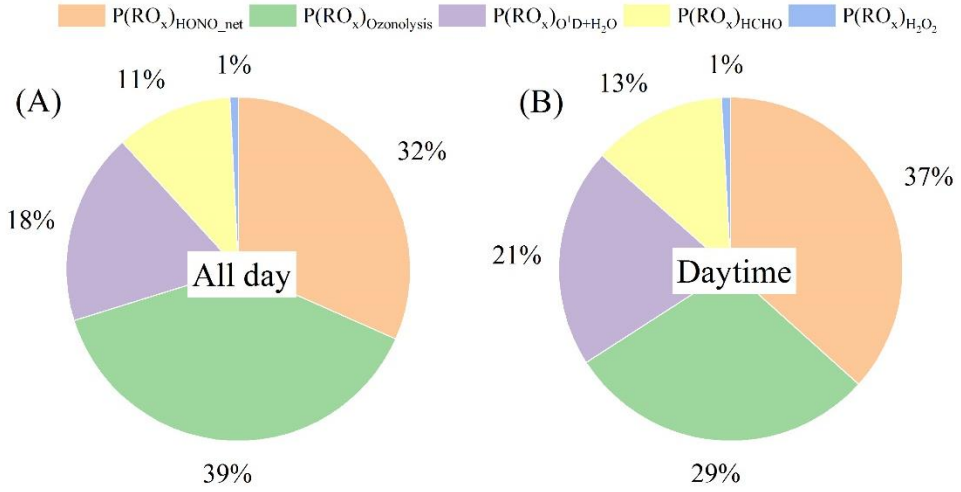


**Figure S11: Relative contributions of different primary $RO_x$ paths (A): throughout the whole day or (B): during the daytime.**

## References


Brown, S. S., Thornton, J. A., Keene, W. C., Pszenny, A. A. P., Sive, B. C., Dubé, W. P., Wagner, N. L., Young, C. J., Riedel, T. P., Roberts, J. M., Vandenboer, T. C., Bahreini, R., Öztürk, F., Middlebrook, A. M., Kim, S., Hübler, G. and Wolfe, D. E.: Nitrogen, Aerosol Composition, and Halogens on a Tall Tower (NACHTT): Overview of a wintertime air chemistry field study in the front range urban corridor of Colorado, J. Geophys. Res. Atmos., 118(14), 8067–8085, doi:10.1002/jgrd.50537, 2013.

Garcia-Nieto, D., Benavent, N. and Saiz-Lopez, A.: Measurements of atmospheric HONO vertical distribution and temporal evolution in Madrid (Spain) using the MAX-DOAS technique, Sci. Total Environ., 643, 957–966, doi:10.1016/j.scitotenv.2018.06.180, 2018.

Jacob, D. J.: Introduction to atmospheric chemistry, Princeton University Press., 1999.

Kleffmann, J., Kurtenbach, R., Lörzer, J., Wiesen, P., Kalthoff, N., Vogel, B. and Vogel, H.: Measured and simulated vertical profiles of nitrous acid - Part I: Field measurements, Atmos. Environ., 37(21), 2949–2955, doi:10.1016/S1352-2310(03)00242-5, 2003.

Meng, F., Qin, M., Tang, K., Duan, J., Fang, W., Liang, S., Ye, K., Xie, P., Sun, Y., Xie, C., Ye, C., Fu, P., Liu, J. and Liu, W.: High-resolution vertical distribution and sources of HONO and $NO_2$ in the nocturnal boundary layer in urban Beijing, China, Atmos. Chem. Phys., 20(8), 5071–5092, doi:10.5194/acp-20-5071-2020, 2020.

Ryan, R. G., Rhodes, S., Tully, M., Wilson, S., Jones, N., Frieß, U. and Schofield, R.: Daytime HONO, $NO_2$ and aerosol distributions from MAX-DOAS observations in Melbourne, Atmos. Chem. Phys. Discuss., (2), 1–27, doi:10.5194/acp-2018-409, 2018.

Seinfeld, J. H. and Pandis, S. N.: Atmospheric Chemistry and Physics: From Air Pollution to Climate Change, John Wiley & Sons., 2016.

Vandenboer, T. C., Brown, S. S., Murphy, J. G., Keene, W. C., Young, C. J., Pszenny, A. A. P., Kim, S., Warneke, C., De Gouw, J. A., Maben, J. R., Wagner, N. L., Riedel, T. P., Thornton, J. A., Wolfe, D. E., Dubé, W. P., Öztürk, F., Brock, C. A., Grossberg, N., Lefer, B., Lerner, B., Middlebrook, A. M. and Roberts, J. M.: Understanding the role of the ground surface in HONO vertical structure: High resolution vertical profiles during NACHTT-11, J. Geophys. Res. Atmos., 118(17), 10,155-10,171, doi:10.1002/jgrd.50721, 2013.

Vogel, B., Vogel, H., Kleffmann, J. and Kurtenbach, R.: Measured and simulated vertical profiles of nitrous acid - Part II. Model simulations and indications for a photolytic source, Atmos. Environ., 37(21), 2957–2966, doi:10.1016/S1352-2310(03)00243-7, 2003.

Wang, Y., Dörner, S., Donner, S., Böhnke, S., De Smedt, I., Dickerson, R. R., Dong, Z., He, H., Li, Z., Li, Z., Li, D., Liu, D., Ren, X., Theys, N., Wang, Y., Wang, Z., Xu, H., Xu, J. and Wagner, T.: Vertical profiles of $NO_2$, $SO_2$, HONO, HCHO, CHOCHO and aerosols derived from MAX-DOAS measurements at a rural site in the central western North China Plain and

their relation to emission sources and effects of regional transport, Atmos. Chem. Phys., 19(8), 5417–5449, doi:10.5194/acp-19-5417-2019, 2019.

Wolfe, G. M., Marvin, M. R., Roberts, S. J., Travis, K. R. and Liao, J.: The framework for 0-D atmospheric modeling (F0AM) v3.1, Geosci. Model Dev., 9(9), 3309–3319, doi:10.5194/gmd-9-3309-2016, 2016.

Xing, C., Liu, C., Hu, Q., Fu, Q., Wang, S., Lin, H., Zhu, Y., Wang, S., Wang, W., Javed, Z., Ji, X. and Liu, J.: Vertical distributions of wintertime atmospheric nitrogenous compounds and the corresponding OH radicals production in Leshan, southwest China, J. Environ. Sci., 105, 44–55, doi:10.1016/j.jes.2020.11.019, 2021.

Xue, C., Ye, C., Zhang, C., Catoire, V., Liu, P., Gu, R., Zhang, J., Ma, Z., Zhao, X., Zhang, W., Ren, Y., Krysztofiak, G., Tong, S., Xue, L., An, J., Ge, M., Mellouki, A. and Mu, Y.: Evidence for Strong HONO Emission from Fertilized Agricultural Fields and its Remarkable Impact on Regional O 3 Pollution in the Summer North China Plain, ACS Earth Sp. Chem., 5(2), 340–347, doi:10.1021/acsearthspacechem.0c00314, 2021.

Ye, C., Zhou, X., Pu, D., Stutz, J., Festa, J., Spolaor, M., Tsai, C., Cantrell, C., Mauldin III, R. L., Weinheimer, A., Hornbrook, R. S., Apel, E. C., Guenther, A., Kaser, L., Yuan, B., Karl, T., Haggerty, J., Hall, S., Ullmann, K., Smith, J. and Ortega, J.: Tropospheric HONO distribution and chemistry in the southeastern US, Atmos. Chem. Phys., 18(12), 9107–9120, doi:10.5194/acp-18-9107-2018, 2018.

Zhang, N., Zhou, X., Shepson, P. B., Gao, H., Alaghmand, M. and Stirm, B.: Aircraft measurement of HONO vertical profiles over a forested region, Geophys. Res. Lett., 36(15), L15820, doi:10.1029/2009GL038999, 2009.